ADVANCED FUNCTIONAL MATERIALS
www.afm-journal.de

Epitaxial Growth of Lead-Free Double Perovskite Shell for $CsPbX_3/Cs_2SnX_6$ (X = Cl, Br, and I) Core/Shell Perovskite Nanocrystals with Enhanced Photoelectric Properties and Stability

*Hanjie Lin, Shuya Li, Yuchen Zhang, Chun Chu, Walker MacSwain, Robert W. Meulenberg, Quinn Qiao, Dong Zhao, and Weiwei Zheng**

All-inorganic lead halide perovskite nanocrystals (NCs) have great optoelectronic properties with promising applications in light-emitting diodes (LEDs), lasers, photodetectors, solar cells, and photocatalysis. However, the intrinsic toxicity of Pb and instability of the NCs impede their broad applications. Shell-coating is an effective method for enhanced environmental stability while reducing toxicity by choosing non-toxic shell materials such as metal oxides, polymers, silica, etc. However, multiple perovskite NCs can be encapsulated within the shell material and a uniform epitaxial-type shell growth of well-isolated NCs is still challenging. In this work, lead-free vacancy-ordered double perovskite Cs_2SnX_6 (X = Cl, Br, and I) shells are epitaxially grown on the surface of $CsPbX_3$ NCs by a hot-injection method. The effectiveness of the non-toxic double perovskite shell protection is demonstrated by the enhanced environmental and phase stability against UV illumination and water. In addition, the photoluminescence quantum yields (PL QYs) increase for the $CsPbCl_3$ and $CsPbBr_3$ NCs after shelling because of the type I band alignment of the core/shell materials, while enhanced charge transport properties obtained from $CsPbI_3/Cs_2SnI_6$ core/shell NCs are due to the efficient charge separation in the type II core/shell band alignment.

1. Introduction

All-inorganic cesium lead halide ($CsPbX_3$, X = Cl, Br, and I) perovskite NCs have extraordinary properties such as tunable bandgaps over the entire visible spectral range, high PL QYs and superior charge transport properties,[1] which are promising for many optoelectronic applications such as LEDs,[2] photodetectors,[3] solar cells,[4] X-ray scintillators,[5] and photocatalysts,[6] etc. However, the soft ionic bonding nature and low crystal lattice energy of perovskite NCs often result in poor stabilities of perovskites against polar solvents, light, moisture, and heat.[7] For example, $CsPbI_3$ can undergo various phase transitions and is very unstable under ambient conditions, even though it is a promising material in many optoelectronic applications due to its large absorption coefficient, small bandgap, and high PL QY.[8] Additionally, the intrinsic toxicity of Pb in lead-based halide perovskites presents serious safety and environmental concerns, which hinders their potential wide range of applications.[9]

To address stability and toxicity issues, encapsulation of perovskite NCs in other more stable and nontoxic materials, such as metal oxides (e.g., AlO_x, TiO_2),[10] polymers,[11] silica[12] and metal–organic frameworks (MOFs)[13] have been developed as the protective shell for the perovskite NCs. Although these surface passivated perovskites NCs exhibit excellent stability, the obtained samples are usually not

H. Lin, S. Li, C. Chu, W. MacSwain, W. Zheng
Department of Chemistry
Syracuse University
Syracuse, NY 13244, USA
E-mail: wzhen104@syr.edu

Y. Zhang, Q. Qiao
Mechanical and Aerospace Engineering
Syracuse University
Syracuse, NY 13244, USA

R. W. Meulenberg
Department of Physics and Astronomy and Frontier Institute for Research in Sensor Technologies
University of Maine
Orono, ME 04469, USA

D. Zhao
Division of Materials Science
Honda Research Institute
San Jose, CA 95134, USA

The ORCID identification number(s) for the author(s) of this article can be found under https://doi.org/10.1002/adfm.202309480

DOI: 10.1002/adfm.202309480

monodispersed resulting from 1) multiple perovskite nanoparticles encapsulated in a single shell and 2) large distribution in shell thickness due to the non-epitaxial shell growth, which could make the application challenging of the non-epitaxially encapsulated perovskite nanocomposites used for practical applications, e.g., nanoscale optical research and biological fields.[14] Therefore, it is highly desirable to grow shell materials epitaxially on the surface of perovskite NCs with nearly uniform shell thickness and size monodispersity.

Careful selection of the shell materials is vital to epitaxially grow crystalline shell lattice(s) on the surface of perovskite NCs. To minimize interfacial strain and lattice distortion in core/shell NCs, it is necessary for the core material and shell material to have the same crystal structure and a small lattice mismatch, typically <15%.[7,15] However, $CsPbX_3$ perovskites have relatively large lattice constants that are generally incompatible with many II–VI group wide-bandgap semiconductors such as ZnO and CdS.[16] In addition, unlike the covalent metal chalcogenide NCs, which can tolerate high temperatures for shell growth (>200 °C),[17] the highly ionic $CsPbX_3$ NCs would undergo an undesirable phase or morphology transformation under such a high reaction temperature. Therefore, to avoid the degradation of the perovskite NC core, it is essential to avoid harsh conditions, such as high temperature and/or polar solvents, during the growth of the shell.[14] To date, a few lead-based perovskite materials, such as Cs_4PbX_6, [18] $CsPb_2Br_5$[11] and $CsPbBr_3$,[2c] are employed as shell materials to epitaxially grow onto the surface of the perovskite NCs. However, the toxicity of Pb from those lead-based materials prevents wide applications of the stable core/shell perovskite NCs.

Replacing Pb^{2+} ions with other non- or less-toxic metal elements for lead-free perovskite NCs is a promising strategy to address the toxicity issue of Pb-based perovskites. Isovalent replacement of Pb(II) by Sn(II)[19] or Ge(II)[20] is a straightforward and effective way to lower the toxicity of Pb-based perovskites. However, these materials suffer from chemical instability due to the easy oxidation of divalent Sn(II) and Ge(II) metal ions into tetravalent metal ions.[21] Recently, double perovskites, with the general formula of $A_2B^{(I)}B^{(III)}X_6$ or $A_2B^{(IV)}X_6$, in which Pb(II) is replaced by heterovalent ions or vacancies such as Cs_2AgInX_6,[22] Cs_2SnX_6,[23] Cs_2AgSbX_6[24] and $Cs_2NaInCl_6$,[25] etc, have been successfully synthesized. These double perovskites have more degrees of freedom in selecting the B site cation elements, decent stabilities, and less toxicity. Some of the double perovskites, such as $Cs_2AgInCl_6$,[26] Cs_2SnCl_6[27,] and $Cs_2NaInCl_6$,[25] are direct bandgap materials and can present high PL QYs. For example, Cs_2SnX_6 emerges as a promising lead-free perovskite for optoelectronic applications such as LED,[27–28] photocatalysis,[29] photodetectors[30] and field effect transistors.[31] Cs_2SnX_6 has a face-centered-cubic (*fcc*) structure, which is the same as the cubic crystal structure of $CsPbX_3$. The Cs_2SnX_6 structure can be obtained by replacing two Pb^{2+} ions in the $CsPbX_3$ lattice with a vacancy and a Sn^{4+} ion, forming a "vacancy-ordered double perovskite".[23,31] Compared to normal ABX_3 perovskites, Cs_2SnX_6 exhibits excellent stabilities against moisture, UV light, and heat due to its higher atomic packing fractions, shorter and stronger B—X bonds, and stable (111) facets without dangling bonds on the surface; resulting in weaker interactions with H_2O molecules and a higher energy barrier for H_2O diffusion.[32] The lattice parameters for Cs_2SnCl_6, Cs_2SnBr_6, and Cs_2SnI_6 are 10.38, 10.99, and 11.62 Å, respectively, which is nearly doubled compared to the lattice parameters for cubic $CsPbCl_3$ (5.61 Å), $CsPbBr_3$ (5.95 Å) and $CsPbI_3$ (6.28 Å). However, the heterostructure of $CsPbX_3/Cs_2SnX_6$ can be regarded as a Cs and X lattice extension as shown in Figure S1 (Supporting Information). In the entire skeleton of the $CsPbX_3/Cs_2SnX_6$ heterostructure, the Cs and X lattice positions remained relatively unaltered, and only B-site ions varied.[11,33] Therefore, the lattice mismatch can be calculated as $(a_{(CsPbX3)} - a_{(Cs2SnX6)}/2)/a_{(CsPbX3)}$. The calculated lattice mismatch for Cl, Br, and I-based core/shell NCs is 7.49%, 7.65%, and 7.48%, respectively, indicating a relatively small lattice mismatch. Therefore, lead-free Cs_2SnX_6 double perovskites could act as a shell material for lead-based halide perovskites owing to a similar crystal structure with ABX_3 perovskites, relatively small lattice mismatch (<10%), nontoxicity, and good stabilities. To the best of our knowledge, using lead-free double perovskites as shell materials to epitaxially passivate the surface of perovskite NCs with enhanced stability and properties has not been explored.

In this work, we developed a facile hot-injection method to epitaxially grow cubic phase vacancy-ordered double perovskite Cs_2SnX_6 on the surface of $CsPbX_3$ NCs. In the case of $CsPbCl_3/Cs_2SnCl_6$ and $CsPbBr_3/Cs_2SnBr_6$ NCs, a type I core/shell structure was formed, and as a result, the PL QY was significantly increased from 8% to 48% for $CsPbCl_3$, and 60% to 85% for $CsPbBr_3$, after shelling, while $CsPbI_3/Cs_2SnI_6$ core/shell NCs show lower PL QY after shelling but enhanced charge transport properties due to the type II core/shell band alignment. To further manipulate the optical properties of the core/shell NCs, we also applied the double perovskite shell-coating method to Mn^{2+} doped $CsPbCl_3$ NCs (i.e., Mn:$CsPbCl_3$ NCs). Mn doping has been shown to be an effective method for regulating the electronic and optical properties of perovskite and metal chalcogenide NCs,[34] which expands the potential applications of core/shell perovskite NCs in LEDs and photocatalysis.[35] The stabilities against polar solvents and light of all the $CsPbX_3/Cs_2SnX_6$ core/shell NCs are effectively enhanced. To our best knowledge, this is the first growth of a lead-free perovskite shell on a lead-based perovskite NCs with tunable optical and electronic properties. In addition, although Cs-lattice extension has been reported for $CsBr/CsPbBr_3$[36] and $CsPbBr_3/Cs_4PbBr_6$ NCs, [18] the $CsPbX_3/Cs_2SnX_6$ core/shell system is the first perovskite-based heterostructure with both Cs and X lattice extension.

2. Result and Discussion

2.1. Synthesis and Structure of $CsPbX_3/Cs_2SnX_6$ Core/Shell NCs

In this work, we coated $CsPbX_3$ NCs with lead-free double perovskite Cs_2SnX_6 through a facile hot-injection method. The detailed synthesis is shown in Scheme 1a (Supporting Information) The $CsPbX_3$ cores were synthesized using a hot-injection method by injecting Cs-oleate solution into hot PbX_2 solution at 180 °C.[37] Then a two-pot method was adopted to grow $CsPbCl_3/Cs_2SnCl_6$ core/shell NCs by purifying the $CsPbCl_3$ core NCs, which were redissolved into fresh solvent and ligands along with $SnCl_4$, followed by the injection of Cs-oleate

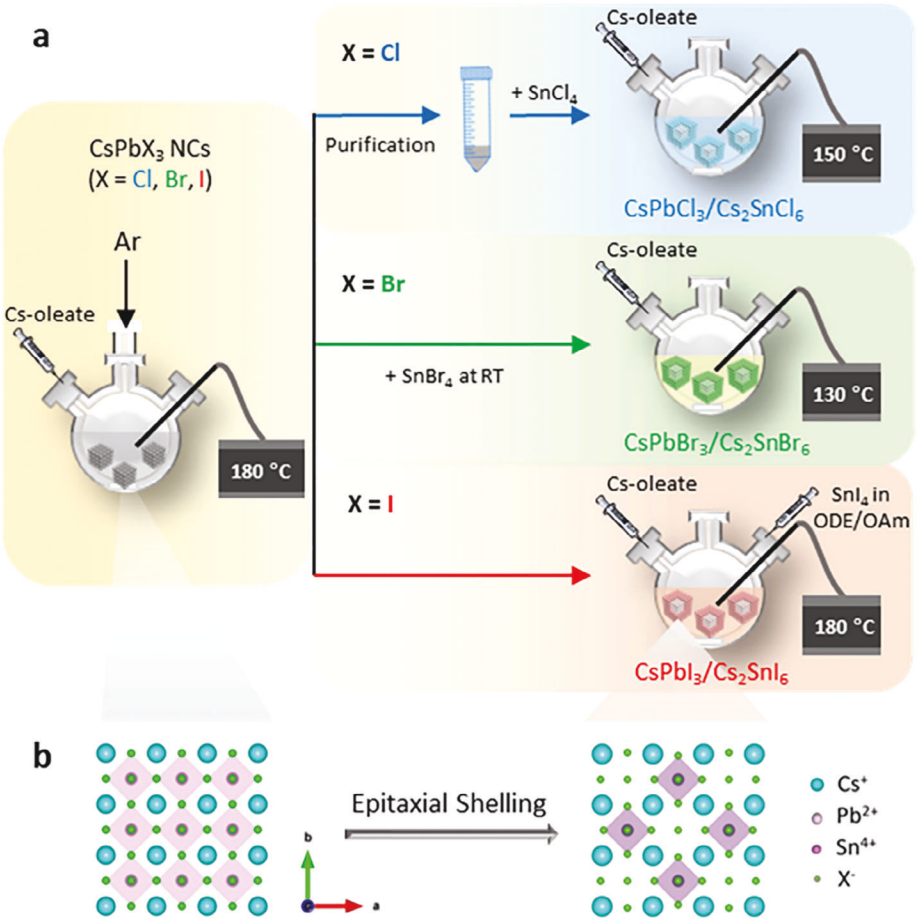

Scheme 1. a) Scheme of the synthesis of $CsPbX_3/Cs_2SnX_6$ NCs. A two-pot shell growth method was used to grow $CsPbCl_3/Cs_2SnCl_6$ core/shell NCs and an one pot shell growth was used to grow $CsPbBr_3$ /Cs_2SnBr_6 , and $CsPbI_3/Cs_2SnI_6$ core/shell NCs. b) Schematic of cubic $CsPbX_3$ (left) and cubic Cs_2SnX_6 lattice (right).

at 150 °C for Cs_2SnCl_6 shell growth. In a control experiment, Cs_2SnX_6 NCs were also synthesized at 220 °C (see details in Supporting Information). The temperature used for shelling reaction is lower than the synthesis of Cs_2SnX_6 NCs due to the presence of $CsPbX_3$ seeds. A one-pot synthesis is used to shell $CsPbI_3$ without purification due to the fast phase transition during the sample cleaning process. In addition, purified $CsPbBr_3$ NCs can undergo side reactions during shell coating indicated by a color change from green to yellow at the beginning of the shell growth. Therefore, the $CsPbI_3$ and $CsPbBr_3$ NCs were not separated from their mother solutions for the shelling process. In addition, it was found that it is important to keep the temperature at 180 °C for the following shelling procedure to prevent phase transition of cubic phase $CsPbI_3$.

Figure 1a–f shows the transmission electron microscopy (TEM) images of $CsPbX_3/Cs_2SnX_6$ core/shell NCs and $CsPbX_3$ cores respectively. The average sizes of $CsPbCl_3$, $CsPbBr_3$, and $CsPbI_3$ core NCs are nanocubes with edges of 9.2 ± 2.2, 7.4 ± 2.0, and 10.2 ± 1.6 nm, respectively (insets of Figure 1a–c), while the average sizes of $CsPbCl_3/Cs_2SnCl_6$, $CsPbBr_3/Cs_2SnBr_6$ and $CsPbI_3/Cs_2SnI_6$ NCs increased to 13.8 ± 3.0, 11.7 ± 3.0, and 13.7 ± 3.0 nm, respectively (insets of Figure 1d–f). The ≈4 nm larger sizes of those core/shell NCs are attributed to the corresponding growth of the double perovskite shell. The high-resolution TEM (HR-TEM) images in the inset of Figure 1d–f clearly shows the core/shell structure with different lattice fringes from the core and shell lattice. The HR-TEM of $CsPbX_3$ core NCs shows the d-spacing of 0.28, 0.30, and 0.31 nm, which correspond to the (200) plane of $CsPbCl_3$, $CsPbBr_3$, and $CsPbI_3$, respectively. The HR-TEM images of $CsPbX_3$/ Cs_2SnX_6 core/shell NCs show different interplanar distances at the core and edge of the core/shell NC. For the $CsPbCl_3/Cs_2SnCl_6$ NCs, a 0.28 nm *d*-spacing in the core region (inset of Figure 1d) is assigned to the (200) plane from $CsPbCl_3$, which is consistent with the TEM image of $CsPbCl_3$ core NCs (inset of Figure 1a). At the edge of the core/shell NC, an interplanar distance of 0.26 nm can be observed for the (400) plane from Cs_2SnCl_6. Similar results were obtained for the $CsPbBr_3/Cs_2SnBr_6$ and $CsPbI_3/Cs_2SnI_6$ core/shell NCs with slightly decreased *d*-spacing from the core (200) plane to the shell (400) plane at the periphery of the NCs (inset of Figure 1e,f). Based on the increased size after shell coating and continuous lattice fringe with slightly decreased *d*-spacing from the core to the periphery of the core/shell NCs, it is reasonable to hypothesize that the (400) plane of Cs_2SnX_6 shell was epitaxially grown on the top of (200) plane of the $CsPbX_3$

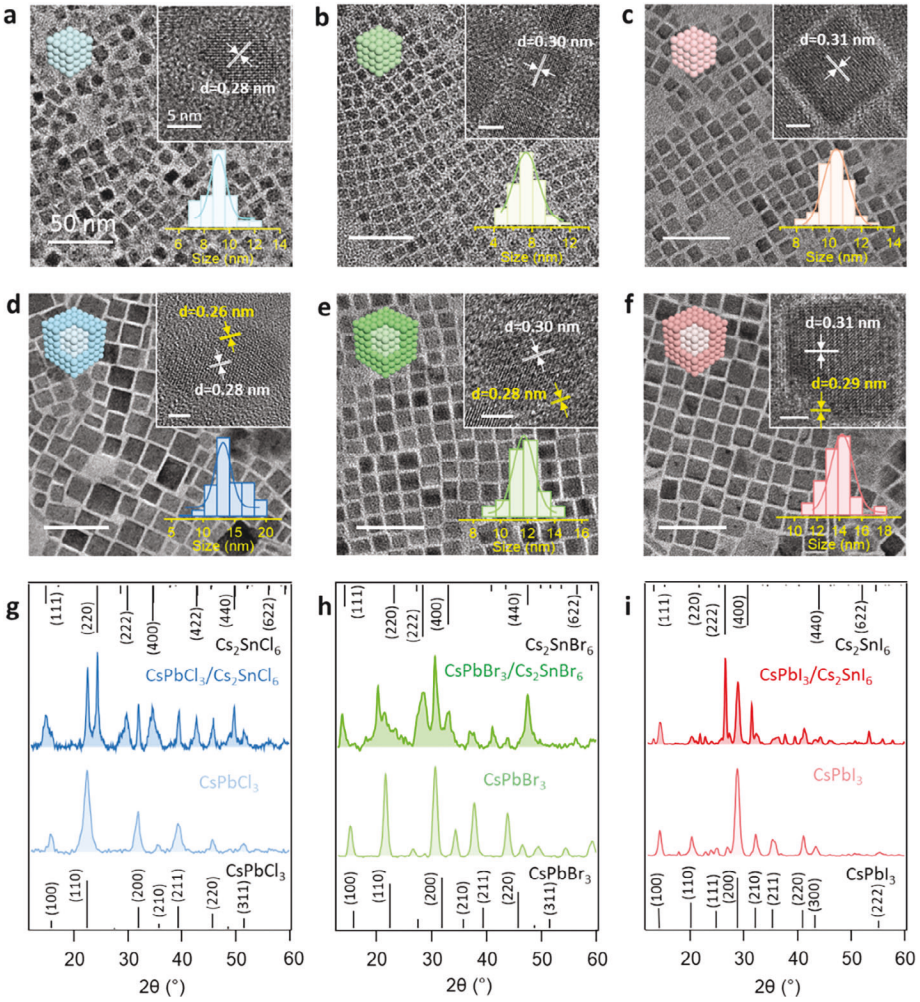

Figure 1. TEM images of a) $CsPbCl_3$, b) $CsPbBr_3$, c) $CsPbI_3$ NCs, d) $CsPbCl_3/Cs_2SnCl_6$, e) $CsPbBr_3/Cs_2SnBr_6$, and f) $CsPbI_3/Cs_2SnI_6$ core/shell NCs. . Insets show HRTEM images: yellow and white marks show the lattice distance of the $CsPbX_3$ core and Cs_2SnX_6 shell, respectively. The scale bar is 5 nm. XRD patterns of g) $CsPbCl_3$ and $CsPbCl_3/Cs_2SnCl_6$, h) $CsPbBr_3$ and $CsPbBr_3/Cs_2SnBr_6$, i) $CsPbI_3$ and $CsPbI_3/Cs_2SnI_6$ NCs.

(Figure S1, Supporting Information). Figure 1g–i presents the X-ray diffraction (XRD) patterns of the $CsPbX_3$ cores and corresponding $CsPbX_3/Cs_2SnX_6$ core/shell NCs, which indicates the cubic phase of the core $CsPbX_3$ NCs. After shell passivation by the lead-free perovskite, new diffraction peaks from cubic phase Cs_2SnX_6 were observed. The peak at 20.10° in the $CsPbBr_3/Cs_2SnBr_6$ XRD pattern is likely from the small amount of side product Cs_4PbBr_6 during the one-pot core/shell synthesis (Figure S2, Supporting Information). Based on the increased size after shell coating from the TEM images and the new XRD peaks from Cs_2SnX_6 after shell coating, it can be concluded that the cubic phase Cs_2SnX_6 shell was epitaxially grown on the top of the $CsPbX_3$ in the $CsPbX_3/Cs_2SnX_6$ core/shell NCs.[16,18]

2.2. Optical Properties

The absorption and PL spectra for the $CsPbX_3$ cores and corresponding $CsPbX_3/Cs_2SnX_6$ NCs are shown in **Figure 2**. The absorption spectra of the core/shell NCs closely resemble those of the core NCs with their absorption peaks shifting from 394 to 660 nm from Cl- to Br- to I-based core/shell NCs.[16] Similarly, the PL peaks for $CsPbCl_3$, $CsPbBr_3$, and $CsPbI_3$ are at 405, 509, and 664 nm, respectively (Figure 2a), which is consistent with the reduction of the bandgap with heavier halide ions in the $CsPbX_3$.[37–38] The absorption spectra of Cs_2SnX_6 NCs are shown in Figure S3 (Supporting Information). For example, the Cs_2SnBr_6 exhibits an absorption peak at ≈350 nm, which is consistent with the reported bandgap of ≈3.5 eV Cs_2SnBr_6.[23,39] This absorption peak ≈350 nm from the Cs_2SnBr_6 could also be observed in the type I core/shell $CsPbBr_3/Cs_2SnBr_6$ NCs as a small hump from ≈2 nm thin Cs_2SnBr_6 shell of the core/shell NCs, confirming the spresence of the Cs_2SnBr_6 shell (Figure 2a). After shelling by the lead-free perovskites, no significant absorption and PL peak shift for $CsPbCl_3/Cs_2SnCl_6$ and $CsPbBr_3/Cs_2SnBr_6$ core/shell NCs was observed. Nevertheless, there was a significant enhancement in the PL QY from 8% to 48% for $CsPbCl_3/Cs_2SnCl_6$ core/shell NCs, and from 60% to 85% for $CsPbBr_3/Cs_2SnBr_6$ core/shell NCs (Figure 2h). The

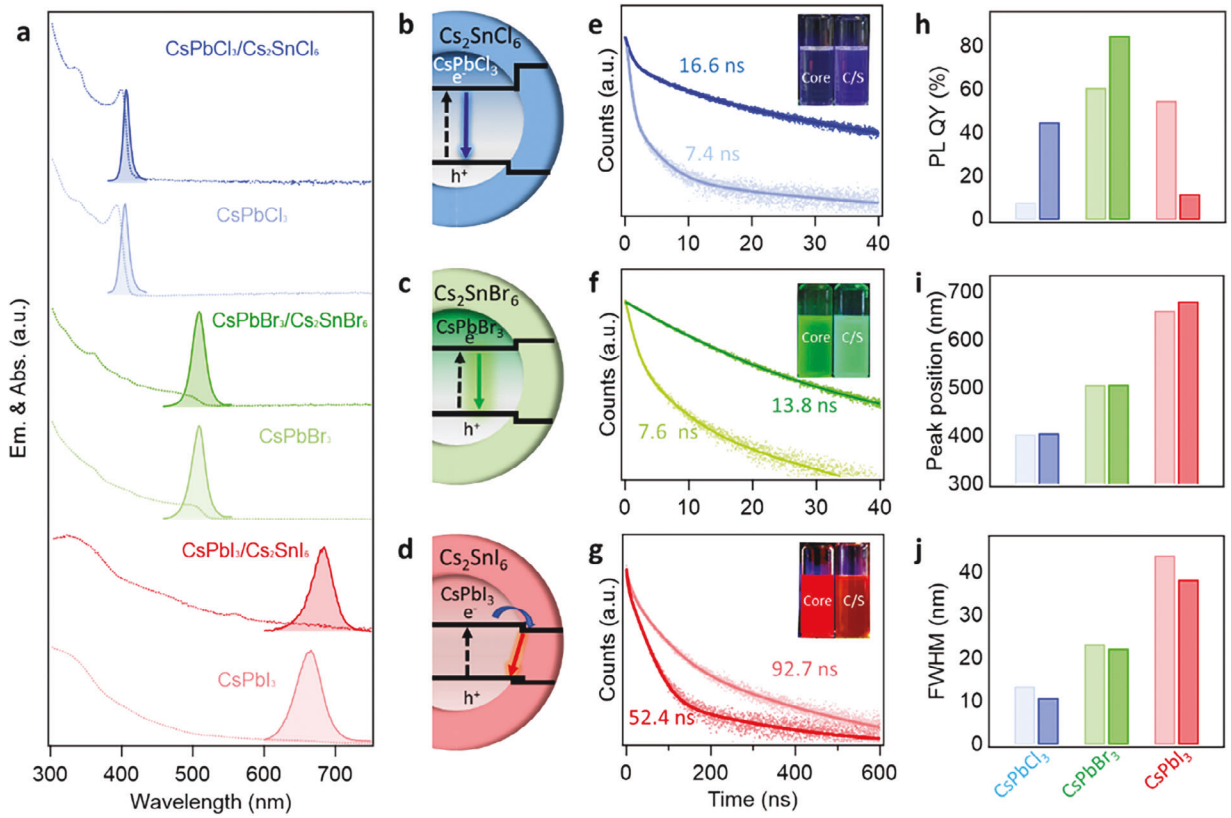

Figure 2. Absorption and PL spectra for a) $CsPbX_3$ NCs and $CsPbX_3/Cs_2SnX_6$ NCs. Schematic illustration of the band structure of b) $CsPbCl_3/Cs_2SnCl_6$, c) $CsPbBr_3/Cs_2SnBr_6$, and d) $CsPbI_3/Cs_2SnI_6$. PL lifetime of e) $CsPbCl_3/Cs_2SnCl_6$ NCs, f) $CsPbBr_3$/Cs2SnBr6 NCs and g) $CsPbI_3/Cs_2SnI_6$ NCs. h) PLQY, i) PL peak position, and j) Full-width half maximum (FWHM) of the PL peaks of $CsPbX_3$ NCs (lighter color) and Cs_2SnX_6 core/shell NCs (darker color).

enhanced PL QY can be understood by the reduced number of surface defects and reduced non-radiative relaxation pathways for excitons (i.e., excited electrons and holes) by shell passivation.[2b] In addition, it has been reported that bulk Cs_2SnCl_6 has a large bandgap of ≈4.5 eV,[39–40], which is much larger than the bandgap of $CsPbCl_3$ (≈3.1 eV, Figure 2b).[41] A similar situation is present in the case of $CsPbBr_3/Cs_2SnBr_6$ NCs; the bandgap of bulk Cs_2SnBr_6 (≈3.5 eV)[39,42] is much larger than the bandgap of bulk $CsPbBr_3$ (≈2.5 eV, Figure 2c). Therefore, a type I core/shell structure is formed in the Cl- and Br-based core/shell perovskite NCs, in which the light-induced excitons are confined in the core.[7,18,43] Additionally, no notable absorption and PL peak shift occurs, indicating the size of the $CsPbBr_3$ and $CsPbCl_3$ core NCs did not change during the shell growth at 130 and 150 °C, respectively (Figure 2i). This result is in contrast with many reported non-epitaxial encapsulation methods, adopting SiO_2[44] or TiO_2[10a] as shell materials, where smaller core perovskite NCs were obtained due to partial sample degradation.

The time-resolved PL (TR-PL) measurements were performed on the core and corresponding core/shell NCs with type I band alignment. The average PL lifetime increases from 7.4 to 16.6 ns after shelling for $CsPbCl_3$ (Figure 2e; Table S1, Supporting Information). Both $CsPbCl_3$ NCs and $CsPbCl_3/Cs_2SnCl_6$ core/shell NCs demonstrate tri-exponential decay in their decay curves. Previous studies have indicated that the fastest and middle decay components can be attributed to trap-mediated non-radiative recombination in the NCs, whereas the slowest decay component is associated with radiative recombination in perovskite NCs.[45] In the case of $CsPbCl_3$ NCs, the fastest and middle decay components accounted for 43.2% and 29.8% of the overall signal, respectively. However, these percentages decreased to 8.5% and 24.6% for $CsPbCl_3/Cs_2SnCl_6$ core/shell NCs, demonstrating the effective elimination of surface defects through the growth of the lead-free perovskite shell. A similar lifetime increase was observed from the $CsPbBr_3$ core NCs with an average lifetime of 7.6 to 13.8 ns for $CsPbBr_3/Cs_2SnBr_6$ core/shell NCs (Figure 2f; Table S1, Supporting Information), which is consistent with the increased PL QYs after shell passivation of the type I core/shell NCs. In addition, the decay of PL of $CsPbBr_3$ cores can be fitted as a tri-exponential decay. However, the $CsPbBr_3/Cs_2SnBr_6$ core/shell NCs exhibit a two-exponential decay behavior, which might indicate the removal of non-irradiative recombination of excitons by the large bandgap lead-free perovskite shell.[46]

For $CsPbI_3/Cs_2SnI_6$ core/shell NCs, the PL peak significantly redshifted from 664 to 684 nm (Figure 2i). The PL QY decreases from 55% to 15% (Figure 2h) and the average PL lifetime decreases from 92.7 to 52.4 ns (Figure 2g; Table S1, Supporting Information) after Cs_2SnI_6 shell coating. The bandgap of bulk Cs_2SnI_6 is ≈1.55 eV,[23,39,47], which is smaller than the bandgap of bulk $CsPbI_3$ (1.8 eV).[41] Therefore, a staggered type II band

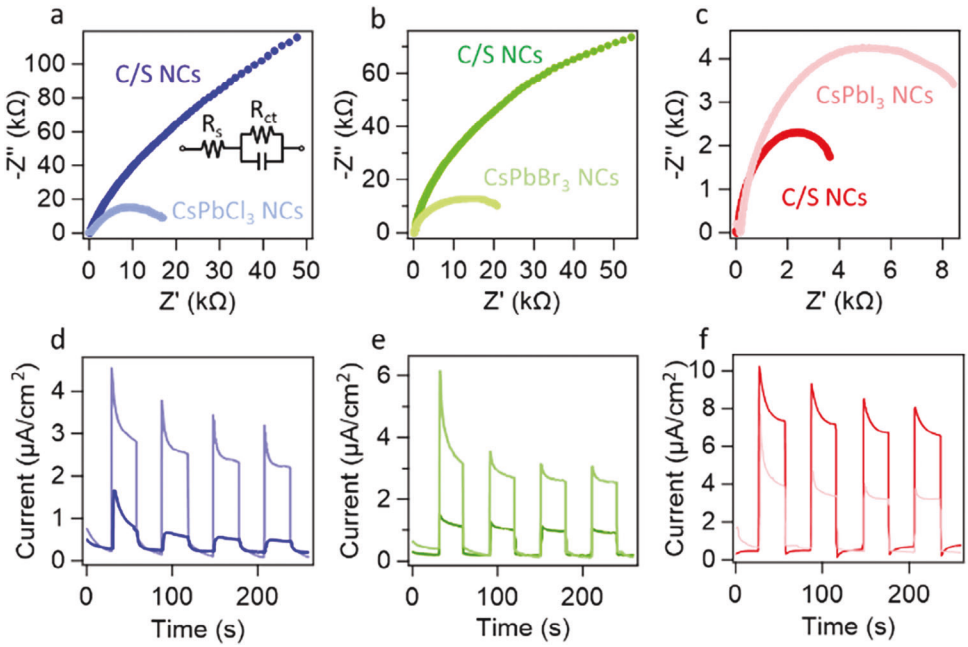

Figure 3. Electrochemical impedance spectra (Nyquist plot) of a) $CsPbCl_3$ and $CsPbCl_3/Cs_2SnCl_6$ (Inset is the equivalent circuit model, and -Z'' and Z' are the virtual and real impedances, respectively), b) $CsPbBr_3$ and $CsPbBr_3/Cs_2SnBr_6$ and c) $CsPbI_3$ and $CsPbI_3/Cs_2SnI_6$ NCs. Transient photocurrent responses to on-off illumination of d) $CsPbCl_3$ and $CsPbCl_3/Cs_2SnCl_6$, e) $CsPbBr_3$ and $CsPbBr_3$/Cs2SnBr$_6$ and f) $CsPbI_3$ and $CsPbI_3/Cs_2SnI_6$ NCs.

alignment was formed in $CsPbI_3/Cs_2SnI_6$ NCs (Figure 2d).[48] The redshift of the PL peaks, the decreased PL QY, and the lower PL lifetime are consistent with charge separation due to the delocalization of electrons to the shell while holes are confined within the core NCs in the type II $CsPbI_3/Cs_2SnI_6$ core/shell NCs.[10a,48,49] It should be noted that the FWHM of PL of the perovskite NCs is smaller after shelling, indicating high-quality core/shell NCs (Figure 2j).

To further manipulate the optical properties of the core/shell NCs, we also applied the double perovskite shell-coating method to Mn^{2+} doped $CsPbCl_3$ NCs (i.e., Mn:$CsPbCl_3$). The detailed synthesis of the Mn:$CsPbCl_3$ and Mn:$CsPbCl_3/Cs_2SnCl_6$ NCs is shown in the Supporting Information. Mn doping has been shown to be an effective method for regulating the electronic and optical properties of perovskite and metal chalcogenide NCs.[34] The XRD pattern for the Mn:$CsPbCl_3$ fits well with the standard cubic phase $CsPbCl_3$, indicating no new phase was formed after introducing the Mn dopants. The XRD pattern of Mn:$CsPbCl_3/Cs_2SnCl_6$ core/shell NCs show both the peaks from $CsPbCl_3$ core and Cs_2SnCl_6 shell, which is consistent with our undoped $CsPbCl_3/Cs_2SnCl_6$ core/shell NCs (Figure S4a, Supporting Information). The TEM images of Mn:$CsPbCl_3$ NCs and Mn:$CsPbCl_3/Cs_2SnCl_6$ NCs are shown in Figure S4e,f (Supporting Information), respectively. The size of the Mn-doped $CsPbCl_3$ NCs increased from 8.2 ± 2.5 nm to 11.5 ± 3 nm after shelling (insets of Figure S4e,f, Supporting Information), supporting a successful growth of a Cs_2SnCl_6 shell on the surface of Mn:$CsPbCl_3$ NCs.

The narrow peak at ≈403 nm from the PL spectra of Mn:$CsPbCl_3$ (Figure S4b, Supporting Information) can be attributed to the band-edge emission from the $CsPbCl_3$ host,[37] and the broad emission centered at 590 nm comes from the ligand field transition ($^4T_1 - ^6A_1$) of Mn^{2+} ions. After shell passivation, the PL QY of Mn:$CsPbCl_3/Cs_2SnCl_6$ was significantly enhanced compared to that of Mn:$CsPbCl_3$ cores from 15% to 58% (Figure S4b, Supporting Information). The lifetime of the host $CsPbCl_3$ excitonic PL ≈403 nm is shorter after doping (from 7.4 to 6.6 ns) due to the exciton energy transfer from the $CsPbCl_3$ host to Mn dopants,[34a] while the lifetime of $CsPbCl_3$ excitonic emissions in core/shell NCs is longer compared to that of Mn:$CsPbCl_3$ cores (from 6.6 to 8.0 ns) due to the removal of the non-radiative recombination pathway caused by surface defects, proving the effective surface passivation of Cs_2SnCl_6[16] (Figure S4c, Supporting Information). The higher PL QY and longer excitonic emission lifetime lead to a reasonable conclusion that the Mn:$CsPbCl_3/Cs_2SnCl_6$ exhibits a type I band alignment as in the $CsPbCl_3/Cs_2SnCl_6$ core/shell NCs.

2.3. Charge Transport Properties

The charge transport properties of the core/shell perovskite NCs were studied through photoelectrochemical analysis. Electrochemical impedance spectroscopy (EIS) Nyquist plots showed a larger semicircle arc for $CsPbCl_3/Cs_2SnCl_6$ and $CsPbBr_3/Cs_2SnBr_6$ than that of corresponding core NCs (**Figure 3**a,b), indicating a higher charge transfer resistance for core/shell NCs upon the formation of a lead-free perovskite shell.[50] This result is consistent with the type I band alignment for Cl- and Br-based core/shell NCs with wider bandgap shell materials compared to that of the core perovskites. In contrast, the semicircle arc for $CsPbI_3/Cs_2SnI_6$ in the Nyquist plot was smaller than that of the $CsPbI_3$ core (Figure 3c), indicating a decreased charge transfer impedance for type II $CsPbI_3/Cs_2SnI_6$

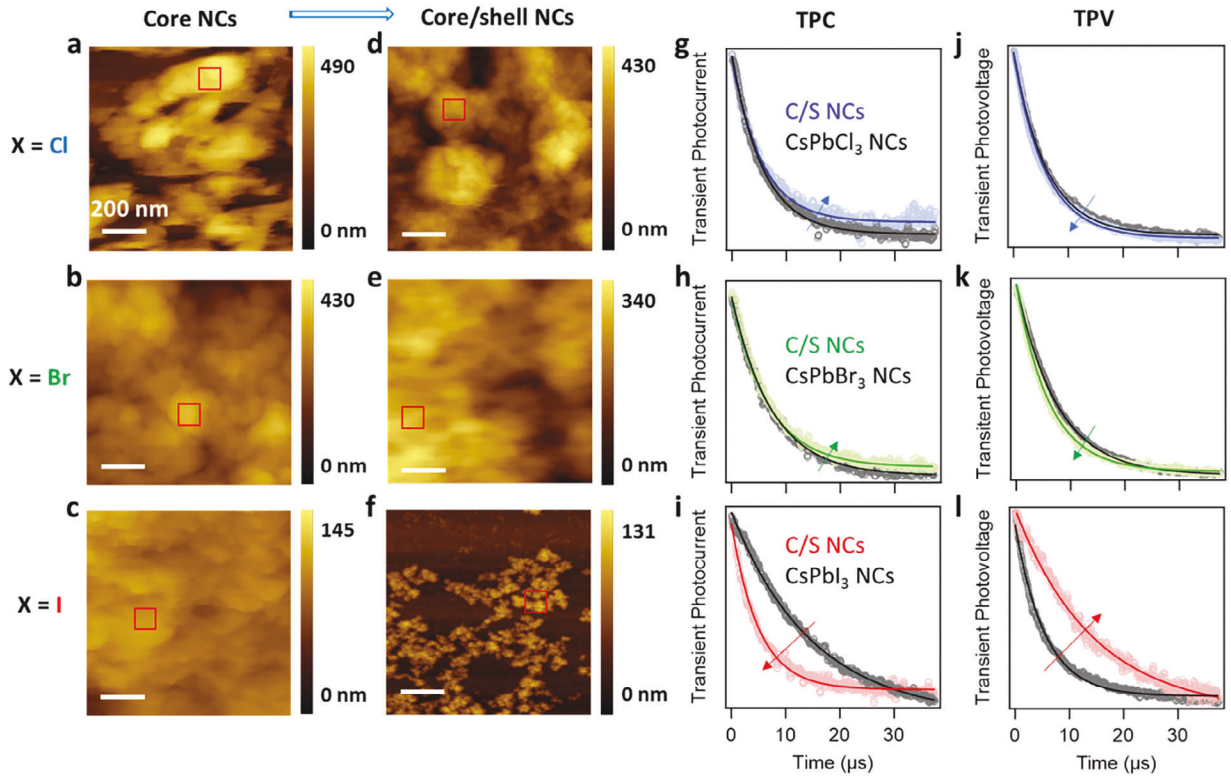

Figure 4. AFM topography images of a) $CsPbCl_3$, b) $CsPbBr_3$, c) $CsPbI_3$ d), $CsPbCl_3/Cs_2SnCl_6$, e) $CsPbBr_3/Cs_2SnBr_6$, and f) $CsPbI_3/Cs_2SnI_6$ NCs. Red squares indicate the areas measured. Normalized TPC decay curve for g) $CsPbCl_3$ and $CsPbCl_3/Cs_2SnCl_6$, h) $CsPbBr_3$ and $CsPbBr_3/Cs_2SnBr_6$ and i) $CsPbI_3$ and $CsPbI_3/Cs_2SnI_6$ NCs. Normalized TPV decay curve for j) $CsPbCl_3$ and $CsPbCl_3/Cs_2SnCl_6$, k) $CsPbBr_3$ and $CsPbBr_3/Cs_2SnBr_6$ and l) $CsPbI_3$ and $CsPbI_3/Cs_2SnI_6$ NCs.

core/shell NCs with the electrons delocalized to the shell and the holes confined in the core.[10a] These band alignment-dependent charge transport properties were further supported by transient photocurrent measurements, which revealed a decrease in photocurrent after shelling for Cl- and Br-based core/shell perovskite NCs (Figure 3d,e), indicating that the photo-generated electrons and holes were confined in the core due to the type I band alignment. In contrast, the photocurrent for $CsPbI_3/Cs_2SnI_6$ NCs increased from ≈4 to ≈7 μA cm^{-2} after shelling (Figure 3f), which can be explained by the type II band alignment with efficient charge separation (Figure 2d).[50]

To further support the band alignment-dependent charge carrier transport properties of the core/shell NCs, conductive atomic force microscopy (C-AFM) was used to measure local transient photocurrent (TPC) and transient photovoltage (TPV) decays. The 100 × 100 nm^2 area, shown by a red square in the AFM topography images (**Figure 4**a–f) was measured for TPC and TPV. The TPC decay curves directly correspond to the material's conductivity and charge mobility.[51] The charge transport lifetimes were measured as 5.47 μs for $CsPbCl_3$, 5.68 μs for $CsPbCl_3/Cs_2SnCl_6$ (Figure 4g), 6.22 μs for $CsPbBr_3$ and 6.55 μs for $CsPbBr_3/Cs_2SnBr_6$ (Figure 4h). The longer charge transport lifetime for core/shell NCs than that of the core NCs is due to the large bandgap shell impeding the electron to transfer between adjacent NCs. In contrast, the charge transport lifetimes were reduced from 14.9 μs for $CsPbI_3$ to 9.47 μs for $CsPbI_3/Cs_2SnI_6$ core/shell NCs (Figure 4i), which indicates the faster charge transport properties as the formation of a type II core/shell structure.

To investigate the charge recombination behavior of the perovskite NCs, the charge carrier lifetime was determined using TPV measurements. A longer charge carrier lifetime indicates a slower recombination rate, which implies a more efficient charge extraction and enhanced charge separation.[51] The charge carrier lifetimes are 5.92 μs for $CsPbCl_3$, 5.77 μs for $CsPbCl_3/Cs_2SnCl_6$ (Figure 4j), 7.27 μs for $CsPbBr_3$ and 6.73 μs for $CsPbBr_3/Cs_2SnBr_6$ (Figure 4k). The shorter charge carrier lifetimes after shelling are likely due to the faster recombination of photo-generated excitons in type I core/shell NCs.[7,18] In contrast, the charge carrier lifetimes were measured as 9.83 μs for $CsPbI_3$ and 14.40 μs for $CsPbI_3/Cs_2SnI_6$. Longer charge carrier lifetimes were observed upon the formation of the Cs_2SnI_6 shell (Figure 4l), due to the type II band alignment, where the holes are confined in the core and the electrons can delocalize to the shell, showing outstanding potential for photoelectrochemical applications.

2.4. Environmental and Phase Stability

To evaluate the stabilities of the core/shell perovskite NCs, first, photo-stability tests of the NCs were performed by placing the samples in toluene under a blue LED (405 ± 15 nm) irradiation with power of 250 ± 40 mW cm^{-2}. The PL of $CsPbX_3$ NCs

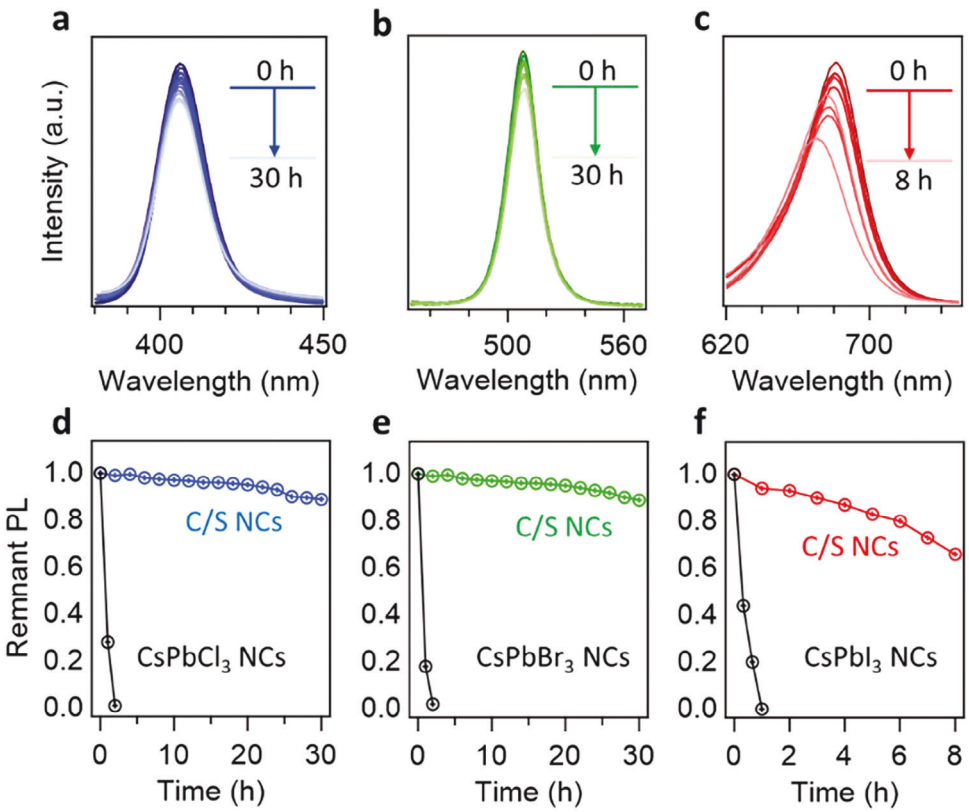

Figure 5. Photo-stability of a) $CsPbCl_3/Cs_2SnCl_6$, b) $CsPbBr_3/Cs_2SnBr_6$, c) $CsPbI_3/Cs_2SnI_6$ core/shell NCs under blue light by monitoring the relative PL intensity of the samples. The comparison of relative PL intensity for d) $CsPbCl_3$ and $CsPbCl_3/Cs_2SnCl_6$, e) $CsPbBr_3$ and $CsPbBr_3/Cs_2SnBr_6$ f) $CsPbI_3$ and $CsPbI_3/Cs_2SnI_6$ NCs.

was completely quenched within 2 h after irradiation from the blue light (Figure S5, Supporting Information). However, the $CsPbCl_3/Cs_2SnCl_6$ and $CsPbBr_3/Cs_2SnBr_6$ remained at 90% and 91% of PL intensity, respectively, after blue light irradiation for 30 h (**Figure 5**a,b,d,e). No obvious peak shift of the core/shell perovskite NCs was observed, indicating no significant sample degradation, which would shrink the size of the NCs and shift the PL peak. In addition, the PL of pure Mn:$CsPbCl_3$ cores was completely quenched within 5 h of exposure to blue light, while the Mn:$CsPbCl_3/Cs_2SnCl_6$ core/shell perovskite NCs retained 88% of their original PL after 30 h of exposure (Figure S6a,b, Supporting Information). Importantly, $CsPbI_3/Cs_2SnI_6$ core/shell NCs also show good environmental stability. It is reported that the cubic phase $CsPbI_3$ is only stable under high temperatures (>175 °C) thermodynamically. At room temperature, it is easy to have a phase transition from cubic phase to orthorhombic non-perovskite phase (yellow phase).[52] This occured to the pure $CsPbI_3$ NCs in our test; after exposure to the LED light for ≈40 min, the black solution started to precipitate out as a yellow powder. The $CsPbI_3$ became completely yellow after 60 min of exposure to the blue light. The corresponding XRD of the yellow phase is shown in Figure S7 (Supporting Information). However, the $CsPbI_3/Cs_2SnI_6$ core/shell NCs maintained its black cubic phase, and no yellow powder was observed; the PL intensity was maintained at 66% of the original PL intensity after exposure to blue light for 8 h (Figure 5c,f). Nevertheless, due to the type II alignment of the $CsPbI_3/Cs_2SnI_6$ NCs with photoexcited electrons delocalized in the shell, as well as the intrinsic instability of $CsPbI_3$, the emission peak blueshifted under the illumination (Figure 5c), indicating partial sample degradation with extended light irradiation.

The water stabilities of the $CsPbX_3/Cs_2SnX_6$ (X = Cl, Br) core/shell NCs were tested by monitoring the PL spectra of the NCs in a solution of hexane mixed in water (**Figure 6**). The PL of $CsPbCl_3$ and $CsPbBr_3$ NCs were completely quenched by storage in water after 1and 5 days, respectively (Figure 6d,e; Figure S8a,b, Supporting Information). However, after being stored in water for 10 days, the PL of $CsPbCl_3/Cs_2SnCl_6$ and $CsPbBr_3/Cs_2SnBr_6$ NCs maintained 68% and 65% of their original PL intensity, respectively. (Figure 6a,b,d,e). Likewise, the water stability of Mn:$CsPbCl_3/Cs_2SnCl_6$ was significantly improved by the lead-free perovskite shell with 72% of the original PL was retained after being stored in water for 10 days, whereas the emission from the unshelled core was completely quenched within one day in water (Figure S6c,d, Supporting Information). Previous reports show that the (222) planes of Cs_2SnCl_6 do not have dangling bonds, which can lead to a higher activation energy for H_2O diffusion into the Cs_2SnCl_6 lattice, which improves the water-resistance of Cs_2SnCl_6.[32] Therefore, we attribute the good water stability of the core/shell perovskite NCs to the (222) planes of Cs_2SnCl_6 shell lattice as well as the short and strong Sn—Cl bonds in Cs_2SnCl_6. The water stability of $CsPbI_3/Cs_2SnI_6$ was also

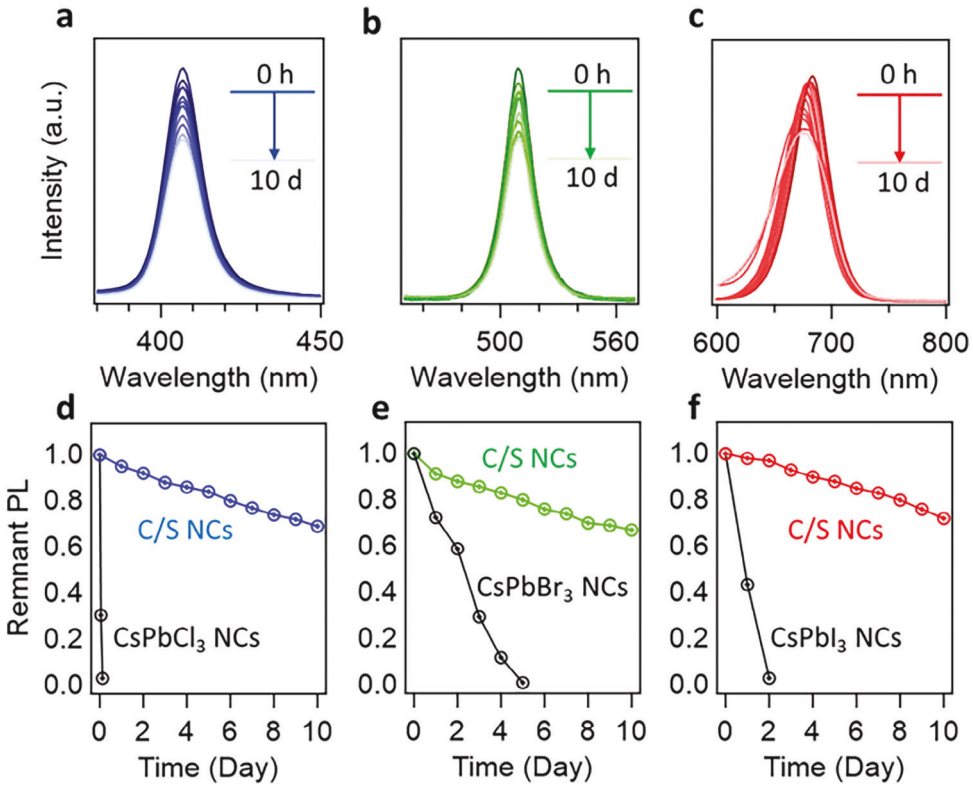

Figure 6. Water-Stability of a) $CsPbCl_3/Cs_2SnCl_6$, b) $CsPbBr_3/Cs_2SnBr_6$, and c) $CsPbI_3/Cs_2SnI_6$ core/shell (C/S) NCs. The comparison of relative PL intensity for d) $CsPbCl_3$ and $CsPbCl_3/Cs_2SnCl_6$, e) $CsPbBr_3$ and $CsPbBr_3/Cs_2SnBr_6$ f) $CsPbI_3$ and $CsPbI_3/Cs_2SnI_6$ NCs.

significantly enhanced compared to that of $CsPbI_3$ core (Figure 6c,f), retaining 70% of the original PL intensity after 10 days in water, despite the emission peak of $CsPbI_3/Cs_2SnI_6$ NCs blueshifting and broadening after water treatment. Conversely, the emission of $CsPbI_3$ NCs was almost totally lost after 2 days in water (Figure S8c, Supporting Information).

The stability in the ambient environment was also tested for $CsPbX_3$ and $CsPbX_3/Cs_2SnX_6$ NCs (Figure S9, Supporting Information). The PL of $CsPbCl_3$ and $CsPbBr_3$ NCs quenched to below 10% and 20% of the original intensity after storing under ambient conditions for 12 weeks, respectively. However, the $CsPbCl_3/Cs_2SnCl_6$ and $CsPbBr_3/Cs_2SnBr_6$ core/shell NCs retained 72% and 89% of the original PL after 12 weeks of storage in air. The $CsPbI_3$ cores experienced a phase transition and the PL quenched completely in 5 days, while the $CsPbI_3/Cs_2SnI_6$ retained the black phase and 70% of the original PL after exposure to air for 22 days. It is believed that the high oxidation state of Sn^{4+} enables the Cs_2SnI_6 to be stable in a wide range of chemical potentials, which protects the unstable $CsPbI_3$ NCs in air/O_2.[30a]

3. Conclusion

In summary, the epitaxial growth lead-free Cs_2SnX_6 double perovskite on the surface of all-inorganic $CsPbX_3$ perovskite NCs for core/shell perovskite NCs has been developed, which presents the first lead-free perovskite shell coated all-inorganic perovskite NCs, reported to date. Significantly, both type I $CsPbX_3/Cs_2SnX_6$ (X = Cl, Br) and type II $CsPbI_3/Cs_2SnI_6$ core/shell perovskite NCs were achieved with tunable optoelectronic properties. The type I $CsPbX_3/Cs_2SnX_6$ (X = Cl, Br) core/shell NCs show enhanced optical properties, including increased PL QYs compared to the $CsPbX_3$ NCs due to the large bandgap protective shell, which confines the photo-induced charge carriers in the core. In contrast, the $CsPbI_3/Cs_2SnI_6$ core/shell NCs show an enhanced charge transport properties evidenced by smaller charger transport impedance, stronger photocurrent, faster TPC, and longer TPV due to the spatial charge separation in the type II $CsPbI_3/Cs_2SnI_6$ core/shell band alignment, which is promising for the potential applications in photocatalysis, solar cell, and photodetector, etc. Furthermore, the stabilities against water, light, and air of the $CsPbX_3/Cs_2SnX_6$ core/shell NCs are effectively enhanced by the shelling, which broadens the applications of perovskite NCs.

4. Experimental Section

Chemicals: Cesium carbonate (Cs_2CO_3, 99.995%, Sigma–Aldrich), lead bromide ($PbBr_2$, 99.999% trace metal, Alfa Aesar), lead chloride ($PbCl_2$, 99.999% trace metal, Alfa Aesar), lead iodide (PbI_2, 99.999%), tin chloride ($SnCl_4$, 99.99%, Alfa Aesar), tin bromide ($SnBr_4$, 99%, Sigma–Aldrich), tin iodide (SnI_4, 99.998%, Fisher), toluene (99.6%, LabChem), oleic acid (OA, 90%, Alfa Aesar), oleylamine (OAm, 70%, Sigma–Aldrich), Trioctylphosphine (TOP, 90%, Thermo Scientific), 1-octadecene (ODE, 90%, Sigma–Aldrich), tetrabutylammonium hexafluorophosphate (≥99.0%, Sigma–Aldrich), acetonitrile (99.5%, VWR), rhodamine 6G

(99%, Fisher), and ethanol (ACS grade, Fisher) were purchased and used without further purification.

Synthesis of Cs-Oleate: Cs_2CO_3 (0.1625 g, 0.5 mmol), 8 mL ODE, and 0.5 mL OA were loaded into a 25 mL-three-neck flask. The mixture was vacuumed for 1 h at 120 °C, and then heated under Ar to 150 °C until all Cs_2CO_3 was dissolved. Note: Cs-oleate precursors should be preheated to ≈100 °C before injection in the following reactions.

Synthesis of $CsPbX_3$ NCs: All-inorganic $CsPbX_3$ perovskite NCs were synthesized based on a literature reported method.[37] In a typical synthesis, 0.188 mmol PbX_2 (54 mg $PbCl_2$ for $CsPbCl_3$, 69 mg $PbBr_2$ for $CsPbBr_3$, or 87 mg PbI_2 for $CsPbI_3$), 5 mL ODE, 0.5 mL OAm and 0.5 mL OA were loaded in a 25 mL-three-neck flask and degassed for 30 min at 100 °C. The mixture was then heated to 180 °C under Ar, and 0.4 mL Cs-oleate was quickly injected. Five seconds later, the reaction was quenched by immersing the flask in a water bath. For $CsPbCl_3$ NCs, an additional 1 mL of TOP was added to the flask at the beginning to solubilize $PbCl_2$. The solution of the reaction of $CsPbCl_3$ NCs was centrifuged at 5 000 rpm for 5 min. The supernatant was decanted, and the NCs in the precipitate were used for the following shelling reaction. Note: direct shelling method in the reaction flash was applied for $CsPbBr_3$ and $CsPbI_3$ NCs without sample cleaning and precipitation (see details in the Synthesis of core/shell NCs below).

Synthesis of $CsPbX_3/Cs_2SnX_6$ Core/Shell NCs (Scheme 1): Two-pot synthesis for $CsPbCl_3/Cs_2SnCl_6$ core/shell NCs. In the case of $CsPbCl_3/Cs_2SnCl_6$ core/shell NCs, two-pot synthesis was applied with a sample purification step for the core NCs before the following shell growth. The as-synthesized $CsPbCl_3$ NCs (2×10^{-5} mmol) were dissolved in 5 mL ODE, 0.2 mL OA, and 0.2 mL OAm by sonification. Then the perovskite solution was loaded into a 25 mL-three-neck flask along with 21 µL $SnCl_4$ (0.188 mmol). The mixture was degassed at 60 °C for 30 min, and then heated to 150 °C. Cs-oleate (0.06 mL) was injected into the flask three times (0.18 mL in total). Each injection was allowed to react for 1 min, followed by the next injection. Then the solution was quenched by a water bath and centrifuged at 5000 rpm for 5 min. The resulted solid NCs were dissolved in ≈3 mL toluene and then crashed out by adding ≈10 mL ethyl acetate, followed by centrifugation at 5 000 rpm for 5 min. The cleaning process was repeated one more time and the solid was redissolved in toluene for further characterization.

One-pot synthesis for Br- and I-based $CsPbX_3/Cs_2SnX_6$ core/shell NCs. Synthesis of $CsPbBr_3/Cs_2SnBr_6$ core/shell NCs was conducted by a one-pot synthesis: After the synthesis of $CsPbBr_3$ core NCs, the reaction solution was cooled down to room temperature. Then 82 mg $SnBr_4$ (0.188 mmol) was added into the flask without purification of the synthesized $CsPbBr_3$ NCs, followed by degassing for 30 min at 80 °C. The mixture was further heated up to 130 °C, and 0.4 mL of Cs-oleate was injected into the mixture. After 1 min reaction, the solution was cooled down by a water bath. The purification process is the same as that for $CsPbCl_3/Cs_2SnCl_6$ NCs.

For the synthesis of $CsPbI_3/Cs_2SnI_6$ core/shell NCs, SnI_4 precursor solution was made by dissolving 118 mg SnI_4 (0.188 mmol) in 2 mL ODE and 0.5 mL OAm at 120 °C. After the synthesis of $CsPbI_3$ core NCs at 180 °C, 2.5 mL of SnI_4 precursor solution and 0.4 mL Cs-oleate solution in two separate syringes were dropwise injected simultaneously into the reaction. The reaction was quenched by water bath 1 min after the injection of shell precursors. The purification process is the same as that for $CsPbCl_3/Cs_2SnCl_6$ NCs.

Characterization: Powder X-ray diffraction (XRD) patterns were taken on a Bruker D2 Phaser with a LYKXEYE 1D silicon strip detector using Cu Kα radiation ($\lambda = 1.5406$ Å). Transmission electron microscopy (TEM) images were obtained on JEM 2100F (operated at an accelerating voltage of 200 kV). The UV–vis absorption measurements were collected on an Agilent Cary 60 spectrophotometer. The photoluminescence (PL) measurements were performed with a Horiba FluoroMax Plus spectrofluorometer. Time-resolved emission measurements were conducted using an Edinburgh FLS-980 spectrofluorometer with a photomultiplier tube (PMT, R928 Hamamatsu) detector. For NC bandgap PL lifetime measurements, the pulsed excitation light (365 nm) was used by an Edinburgh EPL-360 pulsed laser diode operating at a repetition rate of 0.2 MHz. For Mn^{2+} emission lifetime measurements, the pulsed excitation light was generated by an µF2 60 W xenon flashlamp operating at a repetition rate of 20 Hz. For electrochemical impedance spectroscopy (EIS) and photocurrent measurements, a Gamry Interface 1010E electrochemical workstation was used, and the measurements were performed with a single three-electrode setup with the sample electrode as the working electrode, a platinum wire as the counter electrode, and Ag/Ag^+ (0.1 M tetrabutylammonium hexafluorophosphate, $E_{Ag/Ag+} = +0.424$ V vs NHE) as the reference electrode. Local transient photovoltage (TPV) and transient photocurrent (TPC) decays were acquired using Agilent 5500 conductive atomic force microscopy (AFM) in contact mode.

Supporting Information

Supporting Information is available from the Wiley Online Library or from the author.

Acknowledgements

W.Z. acknowledges support from the NSF CAREER (CHE-1944978), NSF IUCRC Phase I grant (2052611), and the Honda Research Institute.

Conflict of Interest

The authors declare no conflict of interest.

Data Availability Statement

The data that support the findings of this study are available from the corresponding author upon reasonable request.

Keywords

charge transport, core/shell structure, environmental stability, lead-free perovskite, perovskite nanocrystals

Received: August 10, 2023
Revised: October 8, 2023
Published online:

[1] Q. A. Akkerman, G. Rainò, M. V. Kovalenko, L. Manna, *Nat. Mater.* **2018**, *17*, 394.
[2] a) G. Pacchioni, *Nat. Rev. Mater.* **2021**, *6*, 108; b) C. Zhang, J. Chen, L. Kong, L. Wang, S. Wang, W. Chen, R. Mao, L. Turyanska, G. Jia, X. Yang, *Adv. Funct. Mater.* **2021**, *31*, 2100438; c) C. Zhang, S. Wang, X. Li, M. Yuan, L. Turyanska, X. Yang, *Adv. Funct. Mater.* **2020**, *30*, 1910582.
[3] C. Li, H. Wang, F. Wang, T. Li, M. Xu, H. Wang, Z. Wang, X. Zhan, W. Hu, L. Shen, *Light Sci Appl* **2020**, *9*, 31.
[4] M. A. Green, A. Ho-Baillie, H. J. Snaith, *Nat. Photonics* **2014**, *8*, 506.
[5] Q. Chen, J. Wu, X. Ou, B. Huang, J. Almutlaq, A. A. Zhumekenov, X. Guan, S. Han, L. Liang, Z. Yi, J. Li, X. Xie, Y. Wang, Y. Li, D. Fan, D. B. L. Teh, A. H. All, O. F. Mohammed, O. M. Bakr, T. Wu, M. Bettinelli, H. Yang, W. Huang, X. Liu, *Nature* **2018**, *561*, 88.
[6] X. Zhu, Y. Lin, J. San Martin, Y. Sun, D. Zhu, Y. Yan, *Nat. Commun.* **2019**, *10*, 2843.
[7] G. H. Ahmed, J. Yin, O. M. Bakr, O. F. Mohammed, *ACS Energy Lett.* **2021**, *6*, 1340.

[8] X. Zhang, M. Lu, Y. Zhang, H. Wu, X. Shen, W. Zhang, W. Zheng, V. L. Colvin, W. W. Yu, *ACS Cent. Sci.* **2018**, *4*, 1352.
[9] H. Tang, Y. Xu, X. Hu, Q. Hu, T. Chen, W. Jiang, L. Wang, W. Jiang, *Adv. Sci.* **2021**, *8*, 2004118.
[10] a) Z.-J. Li, E. Hofman, J. Li, A. H. Davis, C.-H. Tung, L.-Z. Wu, W. Zheng, *Adv. Funct. Mater.* **2018**, *28*, 1704288; b) Y. Ji, M. Wang, Z. Yang, H. Wang, M. A. Padhiar, J. Shi, H. Qiu, A. S. Bhatti, *J. Phys. Chem. C* **2022**, *126*, 1542.
[11] G. Jiang, C. Guhrenz, A. Kirch, L. Sonntag, C. Bauer, X. Fan, J. Wang, S. Reineke, N. Gaponik, A. Eychmüller, *ACS Nano* **2019**, *13*, 10386.
[12] a) W. Shi, X. Zhang, K. Matras-Postolek, P. Yang, *ACS Appl. Nano Mater.* **2021**, *4*, 9391; b) M. Fan, J. Huang, L. Turyanska, Z. Bian, L. Wang, C. Xu, N. Liu, H. Li, X. Zhang, C. Zhang, X. Yang, *Adv. Funct. Mater.* **2023**, *33*, 2215032.
[13] H. He, Y. Cui, B. Li, B. Wang, C. Jin, J. Yu, L. Yao, Y Yang, B. Chen, G. Qian, *Adv. Mater.* **2019**, *31*, 1806897.
[14] Q. Zhong, M. Cao, Q. Zhang, *Nanoscale* **2021**, *13*, 19341.
[15] a) C. Tan, J. Chen, X.-J. Wu, H. Zhang, *Nat. Rev. Mater.* **2018**, *3*, 17089; b) S. Bera, N. Pradhan, *ACS Energy Lett.* **2020**, *5*, 2858.
[16] F. Gao, J. Wu, Y. Zhao, T. Song, Z. Deng, P. Wang, Y. Wang, H. Li, *Nanoscale* **2021**, *13*, 10329.
[17] a) E. Hofman, R. J. Robinson, Z.-J. Li, B. Dzikovski, W. Zheng, *J. Am. Chem. Soc.* **2017**, *139*, 8878; b) Z.-J. Li, E. Hofman, A. Blaker, A. H. Davis, B. Dzikovski, D-K. Ma, W. Zheng, *ACS Nano* **2017**, *11*, 12591.
[18] C. Jia, H. Li, X. Meng, H. Li, *Chem. Commun.* **2018**, *54*, 6300.
[19] T. C. Jellicoe, J. M. Richter, H. F. J. Glass, M. Tabachnyk, R. Brady, S. E. Dutton, A. Rao, R. H. Friend, D. Credgington, N. C. Greenham, M. L. Böhm, *J. Am. Chem. Soc.* **2016**, *138*, 2941.
[20] L. Men, B. A. Rosales, N. E. Gentry, S. D. Cady, J. Vela, *ChemNanoMat* **2019**, *5*, 334.
[21] Q Liu, J. Yin, B.-B. Zhang, J.-K. Chen, Y. Zhou, L-M. Zhang, L-M. Wang, Q. Zhao, J. Hou, J. Shu, B Song, N. Shirahata, O. M. Bakr, O. F. Mohammed, H.-T. Sun, *J. Am. Chem. Soc.* **2021**, *143*, 5470.
[22] J. Luo, S. Li, H. Wu, Y. Zhou, Y. Li, J. Liu, J. Li, K. Li, F. Yi, G. Niu, J. Tang, *ACS Photonics* **2017**, *5*, 398.
[23] A. Veronese, M. Patrini, D. Bajoni, C. Ciarrocchi, P. Quadrelli, L. Malavasi, *Front Chem.* **2020**, *8*, 35.
[24] B. Yang, F. Hong, J. Chen, Y. Tang, L Yang, Y. Sang, X. Xia, J. Guo, H. He, S. Yang, W. Deng, K. Han, *Angew. Chem., Int. Ed.* **2019**, *58*, 2278.
[25] X. Liu, X Xu, B. Li, L. Yang, Q Li, H. Jiang, D. Xu, *Small* **2020**, *16*, e2002547.
[26] B. Yang, X. Mao, F. Hong, W. Meng, Y. Tang, X. Xia, S. Yang, W. Deng, K. Han, *J. Am. Chem. Soc.* **2018**, *140*, 17001.
[27] W. Zhang, W. Zheng, L. Li, P. Huang, Z. Gong, Z. Zhou, J. Sun, Y. Yu, X. Chen, *Angew. Chem., Int. Ed.* **2022**, *61*, e202116085.
[28] Z. Tan, J. Li, C. Zhang, Z. Li, Q. Hu, Z. Xiao, T. Kamiya, H. Hosono, G. Niu, E. Lifshitz, Y. Cheng, J. Tang, *Adv. Funct. Mater.* **2018**, *28*, 1801131.
[29] a) P. Zhou, H. Chen, Y. Chao, Q. Zhang, W. Zhang, F. Lv, L. Gu, Q. Zhao, N. Wang, J. Wang, S. Guo, *Nat. Commun.* **2021**, *12*, 4412; b) X.-D. Wang, Y.-H. Huang, J.-F. Liao, Y. Jiang, L. Zhou, X.-Y. Zhang, H.-Y. Chen, D.-B. Kuang, *J. Am. Chem. Soc.* **2019**, *141*, 13434.
[30] a) X. Han, J. Liang, J.-H. Yang, K. Soni, Q. Fang, W. Wang, J. Zhang, S. Jia, A. A. Martí, Y. Zhao, J. Lou, *Small* **2019**, *15*, e1901650; b) S. Ghosh, S. Paul, S. K. De, *Part. Part. Syst. Charact.* **2018**, *35*, 1800199.
[31] A. Wang, X. Yan, M. Zhang, S. Sun, M. Yang, W. Shen, X. Pan, P. Wang, Z. Deng, *Chem. Mater.* **2016**, *28*, 8132.
[32] Y. Chu, Y. Hu, Z. Xiao, *J. Phys. Chem. C* **2021**, *125*, 9688.
[33] S. K. Dutta, S. Bera, N. Pradhan, *Chem. Mater.* **2021**, *33*, 3868.
[34] a) D. Parobek, B. J. Roman, Y. Dong, H Jin, E. Lee, M. Sheldon, D. H. Son, *Nano Lett.* **2016**, *16*, 7376; b) A. H. Davis, S. Li, H. Lin, C. Chu, J. M. Franck, G. Leem, M. M. Maye, W. Zheng, *J. Mater. Chem. C* **2021**, *9*, 14226.
[35] a) Z.-J. Li, S. Li, A. H. Davis, E. Hofman, G. Leem, W. Zheng, *Nano Res.* **2020**, *13*, 1668; b) F. Locardi, M. Cirignano, D. Baranov, Z. Dang, M. Prato, F. Drago, M. Ferretti, V. Pinchetti, M. Fanciulli, S. Brovelli, L. De Trizio, L. Manna, *J. Am. Chem. Soc.* **2018**, *140*, 12989.
[36] J. Shamsi, Z. Dang, P. Ijaz, A. L. Abdelhady, G. Bertoni, I. Moreels, L. Manna, *Chem. Mater.* **2018**, *30*, 79.
[37] L. Protesescu, S. Yakunin, M. I. Bodnarchuk, F. Krieg, R. Caputo, C. H. Hendon, R. X Yang, A. Walsh, M. V. Kovalenko, *Nano Lett.* **2015**, *15*, 3692.
[38] A. Swarnkar, R. Chulliyil, V. K. Ravi, M. Irfanullah, A. Chowdhury, A. Nag, *Angew. Chem., Int. Ed.* **2015**, *54*, 15424.
[39] M. M. S. Karim, A. M. Ganose, L. Pieters, W. W. Winnie Leung, J. Wade, L. Zhang, D. O. Scanlon, R. G. Palgrave, *Chem. Mater.* **2019**, *31*, 9430.
[40] Z. Tan, Y. Chu, J. Chen, J. Li, G. Ji, G. Niu, L. Gao, Z. Xiao, J. Tang, *Adv. Mater.* **2020**, *32*, 2002443.
[41] V. K. Ravi, G. B. Markad, A. Nag, *ACS Energy Lett.* **2016**, *1*, 665.
[42] C.-F. Lai, Y-C. Chang, Y-C. Tien, *ACS Appl. Nano Mater.* **2021**, *4*, 1924.
[43] L. Kong, X. Zhang, C. Zhang, L. Wang, S. Wang, F. Cao, D. Zhao, A. L. Rogach, X. Yang, *Adv. Mater.* **2022**, *34*, 2205217.
[44] Q. Zhong, M. Cao, H. Hu, D Yang, M. Chen, P. Li, L. Wu, Q. Zhang, *ACS Nano* **2018**, *12*, 8579.
[45] J. Zhang, H. Wang, F. Cao, S. Wang, J. Wu, Y. Dou, J. Zhang, J. Chen, D. Zhao, X. Yang, *Adv. Opt. Mater.* **2019**, *8*, 1900567.
[46] V. K. Ravi, S. Saikia, S. Yadav, V. V. Nawale, A. Nag, *ACS Energy Lett.* **2020**, *5*, 1794.
[47] D. S. Dolzhnikov, C. Wang, Y. Xu, M. G. Kanatzidis, E. A. Weiss, *Chem. Mater.* **2017**, *29*, 7901.
[48] H. Huang, H. Yuan, K. P. F. Janssen, G. Solís-Fernández, Y. Wang, C. Y. X. Tan, D. Jonckheere, E. Debroye, J. Long, J. Hendrix, J. Hofkens, J. A. Steele, M. B. J. Roeffaers, *ACS Energy Lett.* **2018**, *3*, 755.
[49] Z.-J. Li, X.-B. Fan, X-B. Li, J.-X. Li, F. Zhan, Y Tao, X. Zhang, Q.-Y Kong, N.-J. Zhao, J.-P. Zhang, C. Ye, Y-J Gao, X-Z. Wang, Q.-Y. Meng, K Feng, B. Chen, C.-H. Tung, L.i-Z. Wu, *J Mater Chem* **2017**, *5*, 10365.
[50] Y.-F. Xu, M.u-Z.i Yang, B.-X. Chen, X.-D. Wang, H.-Y. Chen, D.-B. Kuang, C.-Y. Su, *J. Am. Chem. Soc.* **2017**, *139*, 5660.
[51] a) E. T. Vickers, T. A. Graham, A. H. Chowdhury, B. Bahrami, B. W. Dreskin, S. Lindley, S. B. Naghadeh, Q. Qiao, J. Z. Zhang, *ACS Energy Lett.* **2018**, *3*, 2931; b) E. T. Vickers, E. E. Enlow, W. G. Delmas, A. C. Dibenedetto, A. H. Chowdhury, B. Bahrami, B. W. Dreskin, T. A. Graham, I. N. Hernandez, S. A. Carter, S. Ghosh, Q. Qiao, J. Z. Zhang, *ACS Energy Lett.* **2020**, *5*, 817.
[52] a) W. J. Mir, A. Alamoudi, J. Yin, K. E. Yorov, P. Maity, R. Naphade, B. Shao, J. Wang, M. N. Lintangpradipto, S. Nematulloev, A.-H. Emwas, A. Genovese, O. F. Mohammed, O. M. Bakr, *J. Am. Chem. Soc.* **2022**, *144*, 13302; b) Z.-J. Li, E. Hofman, A. H. Davis, M. M. Maye, W. Zheng, *Chem. Mater.* **2018**, *30*, 3854.